The Structure of PTP-1B in Complex with a Peptide Inhibitor Reveals an Alternative Binding Mode for Bisphosphonates†

Ernest Asante-Appiah,*,‡ Sangita Patel,§ Claude Dufresne,|| Patrick Roy,|| Qingping Wang,‡ Vira Patel,‡ Richard W. Friesen,|| Chidambaram Ramachandran,‡ Joseph W. Becker,§ Yves Leblanc,|| Brian P. Kennedy,‡ and Giovanna Scapin*,§

Department of Biochemistry and Molecular Biology and Department of Medicinal Chemistry, Merck Frosst Center for Therapeutic Research, Pointe-Claire - Dorval H9R 4P8, Canada, and Department of Medicinal Chemistry, Merck Research Laboratory, Rahway, New Jersey 07065

Received April 11, 2002; Revised Manuscript Received May 15, 2002

ABSTRACT: Inhibitors of PTP-1B could be therapeutically beneficial in the treatment of type 2 diabetes. Owing to the large number of phosphatases in the cell, inhibitors against PTP-1B must not only be potent but selective as well. N-Benzoyl-L-glutamyl-[4-phosphono(difluoromethyl)]-L-phenylalanine-[4-phosphono-(difluoro-methyl)]-L-phenylalanineamide (BzN−EJJ−amide) is a low nanomolar inhibitor of PTP-1B that shows selectivity over several protein tyrosine phosphatases. To gain an insight into the basis of its potency and selectivity, we evaluated several analogues of the inhibitor and introduced amino acid substitutions into PTP-1B by site-directed mutagenesis. We also determined the crystal structure of PTP-1B in complex with BzN−EJJ−amide at 2.5 Å resolution. Our results indicate that the high inhibitory potency is due to interactions of several of its chemical groups with specific protein residues. An interaction between BzN−EJJ−amide and Asp48 is of particular significance, as substitution of Asp48 to alanine resulted in a 100-fold loss in potency. The crystal structure also revealed an unexpected binding orientation for a bisphosphonate inhibitor on PTP-1B, where the second difluorophosphonomethyl phenylalanine (F_2PMP) moiety is bound close to Arg47 rather than in the previously identified second aryl phosphate site demarked by Arg24 and Arg254. Our results suggest that potent and selective PTP-1B inhibitors may be designed by targeting the region containing Arg47 and Asp48.

Diabetes is increasingly becoming an epidemic not only in industrialized countries but in developing nations as well. 300 million people worldwide are predicted by the World Health Organization (WHO) to become diabetic by the year 2025 if current trends continue (*1*). Hence, the need for effective therapies for this disease cannot be overemphasized. Although the causes of diabetes are not clearly understood and appear to be multifactorial, insulin resistance seems to be an underlying factor in the progression of the disease. Attempts to reverse this physiological condition would thus go a long way toward ameliorating the disease. Recent therapies, including the thiazolidinediones that target PPARγ[1] and act as insulin-sensitizers, have been found to be quite efficacious against diabetes (*2*). Another target that is receiving tremendous attention as a candidate for the development of drugs against diabetes is PTP-1B (*3*).

Mice lacking PTP-1B are insulin-sensitive and maintain euglycemia in the fed state with half the amount of circulating insulin found in wild-type litter mates. The PTP-1B -/- mice also show an enhanced insulin-dependent receptor phosphorylation in glucose-metabolizing tissues such as muscle and liver compared to wild-type litter mates. In addition to their sensitivity to insulin, PTP-1B -/- mice are resistant to diet-induced obesity when fed with a high-fat diet (*4*). Studies with a second knock-out mouse of PTP-1B that was generated differently have corroborated these results (*5*). The current hypothesis posits that PTP-1B plays a key role in dephosphorylation of the insulin receptor; thereby, PTP-1B inhibition should stimulate insulin signaling. Thus, PTP-1B is an attractive candidate for the design of drugs for the treatment of type 2 diabetes and obesity.

Several groups have reported syntheses of inhibitors of PTP-1B (*7*−*16*). A strategy that has yielded potent inhibitors

† The facilities of the Industrial Macromolecular Crystallography Association Collaborative Access Team (IMCA-CAT) at the Advanced Photon Source are supported by the companies of the Industrial Macromolecular Crystallography Association through a contract with Illinois Institute of Technology (IIT), executed through IIT's Center for Synchrotron Radiation Research and Instrumentation. Use of the Advanced Photon Source was supported by the U. S. Department of Energy, Basic Energy Sciences, Office of Science, under Contract No. W-31-109-Eng-38.

* Corresponding authors. E-mails: Ernest_Asanteappiah@Merck.com, Giovanna_Scapin@Merck.com.

‡ Department of Biochemistry and Molecular Biology, Merck Frosst Center for Therapeutic Research.

§ Department of Medicinal Chemistry, Merck Research Laboratory.

|| Department of Medicinal Chemistry, Merck Frosst Center for Therapeutic Research.

[1] Abbreviations: F_2PMP, difluoro-phosphonomethyl phenylalanine; RMSD, root-mean-squared deviation; DMH, N,N′dimethyl bis(mercaptoacetyl)-hydrazine; IPTG, isopropyl-1-thio-β-D-galactopyranoside; BzN−EJJ−amide, (N-benzoyl-L-glutamyl-[4-phosphono(difluoromethyl)]-L-phenylalanine-[4-phosphono(difluoro-methyl)]-L-phenylalanine-amide; FDP, fluorescein diphosphate; pNPP, para-nitrophenyl phosphate; PTP-1B, protein tyrosine phosphatase-1B.; TCPTP, T-cell protein tyrosine phosphatase; PCR, polymerase-chain reaction; PPARγ, peroxisome-proliferator activated receptor γ.

10.1021/bi0259554 CCC: $22.00
Published on Web 06/25/2002

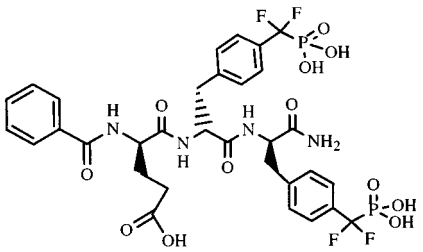

FIGURE 1: Chemical structure of BzN−EJJ−amide.

has involved the substitution of the phenolic oxygen of the tyrosine phosphate with a nonhydrolyzable difluoromethylene group (*17*). It has also been suggested, on the basis of the structure of phosphotyrosine bound to PTP-1B (*18*), that potent and selective PTP-1B inhibitors may be obtained by targeting both the catalytic site as well as a second aryl phosphate-binding site that is found in the protein. This hypothesis is supported by the recently reported crystal structure of PTP-1B in complex with a peptide derived from the insulin receptor (*19*). The structure revealed that the tyrosine phosphates of the peptide occupy both the active site (or primary site) and the secondary aryl phosphate site (identified by Arg24 and Arg254), thus suggesting that the enzyme achieves substrate selectivity by utilizing this secondary phosphate site that is largely absent in other phosphatases.

We recently reported chemical and biological data on BzN−EJJ−amide, a potent and selective inhibitor of PTP-1B and TCPTP containing two non-hydrolyzable phosphate replacements (*20*, *21*). Compounds in this class show at least 30-fold selectivity over several PTPs, including PTPα, SHP-1, SHP-2, and LAR, and are 3 orders of magnitude more selective over cdc25, a dual-specificity phosphatase. BzN−EJJ−amide (Figure 1) contains two negatively charged difluorophenylmethylene phosphonates and a glutamic acid. In our previous report, we suggested that one of the F_2PMP groups would be expected to bind at the active site. Although the crystal structure of PTP-1B in complex with the insulin receptor peptide seemed to suggest that the second moiety could bind at the secondary site, it was not possible by modeling alone to predict the binding orientation of the inhibitor. This uncertainty arose from the presence of two additional negatively charged groups on the inhibitor, either of which could bind to the positively charged secondary binding region. Additionally, mutation of Arg24 (a component of the secondary binding site) to Ala did not significantly abrogate the inhibitory potency of BzN−EJJ−amide on PTP-1B (*20*). To gain an insight into the basis of potency and selectivity of BzN−EJJ−amide and to assess its correct binding mode, we have now determined the crystal structure of the compound in complex with PTP-1B. We have also evaluated several of its analogues and introduced amino acid substitutions into PTP-1B by site-directed mutagenesis. Our results show an unexpected binding mode for the second F_2-PMP moiety and the glutamic acid and allow the identification of the residues most responsible for inhibitor potency and selectivity. Our results reveal significant implications for the design of potent and selective PTP-1B inhibitors.

EXPERIMENTAL PROCEDURES

Mutagenesis and Protein Expression. A plasmid that expresses the isolated catalytic domain of PTP-1B(1−320) in a pFLAG2 vector was used as template DNA for site-directed mutagenesis. A PCR-based approach was used to introduce amino acid substitutions into PTP-1B by following established procedures (*22*). The following mutagenic forward (F) and reverse (R) primers were used for the introduction of mutations into PTP-1B as indicated. R47K-(F): 5′CCGAAATAGGTACAAAGACGTCAGTCCCTTT-GACC3′ R47K-(R) 5′GGTCAA-AGGGACTGACGTCTTTG-TACCTATTTCGG 3′ D48N-(F) 5′ CCGAAATAGGTAC-AGAAACGTCAGTCC−CTTTGACC 3′ D48N-(R) 5′ GGT-CAAAGGGACTGACGTT-TCTGTACCTATTTCGG 3′ D48A-(F) 5′ CCGAA-ATAGGTACAGAGCCGTCAGTC−CCTTTGACC 3′ D48A-(R) 5′ GGTCAAAGGGACTGACG-GCTCTGTACCTATTTC-GG 3′. The correct construction of mutants was verified by DNA sequencing on an ABI 373 DNA sequencer (Applied Biosystems). The sequence data were analyzed by the software application package Sequencher 4.0.5 (Gene Code Corp.).

Following confirmation of the desired mutations, DNA was transformed into *Escherichia coli* BL21 cells for verification of protein expression. Protein expression was assessed by growing transformed *E. coli* cells to an absorbance of ∼0.7 units at 600 nm in Luria Bertani broth. Upon induction of the culture with 1 mM IPTG for 2 h, cells were harvested by centrifugation. Cell lysate was analyzed by electrophoresis on a 10−20% polyacrylamide gel containing sodium dodecyl sulfate (SDS−PAGE). Protein was transferred onto nitrocellulose, blotted with an anti-FLAG monoclonal antibody, and detected by chemiluminescence. The SuperSignal west pico kit was used for immunoblotting of proteins by following the suggested protocol (Pierce). Wild-type PTP-1B and mutant derivatives were purified as reported previously (*20*).

Activity Assays. The activities of wild-type PTP-1B and mutant derivatives were assayed with *p*-nitrophenolphosphate (pNPP) and fluorescein diphosphate (FDP) as substrates. The assays were carried out in a 96-well plate at room temperature in a buffer consisting of 20 mM Bis-Tris, 5 mM DMH, 2 mM EDTA, 5% (v/v) DMSO, 2% (v/v) glycerol, 0.01% (v/v) Triton X-100, at a pH of 6.3. An end-point assay was employed for hydrolysis of pNPP. Following a 5 min incubation, the reaction was stopped with 0.1M NaOH and absorbance at 405 nm measured. Hydrolysis of FDP was monitored continuously on a Cytofluor microplate reader. Excitation and emission wavelengths were set at 440 and 515 nm, respectively. Kinetic constants were determined by fitting observed rates of reactions to the Michaelis−Menten equation with the aid of the nonlinear curve fitting software program, Grafit 4.0.10 (Erithacus, software Inc.). Similarly, inhibition concentrations that result in 50% inhibition of enzyme activity (IC_{50}) values were derived by fitting rates obtained in the presence and absence of compounds to a four-parameter equation using Grafit. A substrate concentration that was equivalent to the K_M value of the enzyme derivative was used for IC_{50} determinations. The enzyme concentrations of PTP-1B derivatives were normalized to give 10 arbitrary fluorescence units/sec for IC_{50} determinations. The average of at least three determinations of the kinetic parameters ± the standard deviation is reported. The methods for the synthesis of compounds have been published previously (*6*).

Crystallization and Data Collection. On the basis of the fact that residues 285−295 are often disordered in many

Table 1: Statistics for the Data Used to Solve the Structure of the FLAG-PTP-1B(1−283):BzN−EJJ−Amide Complex[a]

space group	C2
unit cell parameters	$a = 186.87$ Å, $b = 154.42$ Å, $c = 64.60$ Å $\beta = 94.56°$
molecule/au	4
resolution range (Å)	30−2.5
no. of observations	176274 (17193)
no. of reflections	61097 (9039)
completeness (%)	96.9 (86.4)
$\langle I/\sigma I \rangle$	6.0 (1.5)
R_{merge} (I)	12.1 (38.0)

[a] Numbers refer to all data with $I/\sigma I > 0.0$. Numbers in parentheses represent measurements in the last shell of resolution (2.65−2.5 Å).

PTP-1B structures reported at the start of this study (e.g., pdb entries 2HNQ, 2HNP, 1A5Y), a shorter construct (FLAG-1−283) was used for crystallization experiments. Crystals of FLAG−PTP-1B (1−283) in complex with (BzN−EJJ−amide) were grown by vapor diffusion in sitting drops at 4 °C by mixing 2 μL of protein (5 mg/mL in 20 mM Hepes, pH 7.0, 50 NaCl, 1mM EDTA, 2 mM DMH, 2:1 ration of BzN−EJJ−amide) and 2 μL of precipitant solution (14% PEG 4000, 10% propanol, 100 mM Citrate pH 5.9). Microseeding and reservoir stepping (to 16% PEG 4000, 8% propanol) were necessary to produce larger crystals. X-ray diffraction data were collected on a Mar CCD from a single, bipyramidal crystal (of approximately 0.1 × 0.1 × 0.15 mm in size) using synchrotron radiation. Data were collected at beamline 17-ID in the facilities of the Industrial Macromolecular Crystallography Association Collaborative Access Team (IMCA-CAT) at the Advanced Photon Source (Argonne National Laboratory, Argonne IL). The crystal was soaked in cryoprotectant solution (10% glycerol in mother liquor) for several hours before flash-freezing in the liquid nitrogen stream. A preliminary indexing of the data with HKL2000 (*23*) showed that the crystal is monoclinic, C-centered, with unit cell parameters $a = 186.87$ Å, $b = 154.42$ Å, $c = 64.60$ Å, and $\beta = 94.56°$. All further data processing, scaling, and merging were done with X-GEN (*24*). The calculated unit cell volume is 1 858 131 Å^3. The monomeric molecular weight of the protein used in the crystallographic studies is 34 403 Da, and assuming four molecules per asymmetric unit, we obtained a Vm ratio (*25*) of 3.4 Å^3/Da, corresponding to a solvent content of about 70%, within the range expected for globular protein. Table 1 summarizes the statistics for the data collected.

Structure Solution and Refinement. The three-dimensional structure of the FLAG-PTP-1B(1−283):BzN−EJJ−amide complex was solved by Molecular Replacement techniques, using as search model the 1.8 Å structure of the mutant enzyme in complex with phosphotyrosine (PDB code 1PTY). Bound ligand, solvent molecules, and protein residues 284−298 (C-terminus), and 175−185 (WPD loop) were not included in the search model. Rotation and translation functions were calculated using AMORE (*26*). The four monomers were identified without ambiguity. A noncrystallographic symmetry (NCS) matrix was calculated from the model and applied during the initial stages of refinement. The model was subjected to 30 cycles of rigid body refinement as implemented in XPLOR (*27*, *28*) using data between 8.0 and 2.8 Å, with a 2σ cutoff. 5% of the data were set aside for R_{free} calculation (*29*−*31*) and the rigid-body fitted model was subjected to a cycle of simulated annealing (slow cool) followed by temperature factor refinement. The resulting model had a crystallographic R-factor of 28.9% and an R_{free} of 33.8%. Initial difference Fourier electron density maps calculated from this model clearly showed that, in all four molecules in the AU, the WPD loop was in a closed conformation, and density was visible for the bound inhibitor. The WPD loops were built into the available density using the graphic software O (*32*, *33*).

Refinement of the model was carried out by alternating cycles of manual rebuilding in O and with the aid of computer-based refinement using XPLOR while slowly increasing the resolution to 2.6 Å. Difference Fourier electron density maps unambiguously showed the location and the orientation of the bound inhibitor (Figure 2), and the inhibitor molecules were added to the model. At this point, analysis of the diffraction data with the program TRUNCATE (CCP4,(*34*) and in CNX (*35*), MSI) indicated pseudomerohedral twinning of the data. The twinning operator was defined as (h, $-k$, $-l$), i.e., a 2-fold rotation about the a axis (made possible by the fact that beta is close to 90°), and the twinning fraction was estimated to be 4.4%. The refinement was continued with CNX, using all available data between 30 and 2.5 Å. Typically, two cycles of torsion angle dynamics (*36*), positional, and temperature factor refinements were run in each cycle. Bulk solvent correction was applied throughout the entire refinement. The current model has a crystallographic R-factor of 22.8% and an R_{free} of 28.6% for 61052 reflections between 30.0 and 2.5 Å (97% of possible; 5% flagged for R_{free} calculation) and maintains good geometry (rmsd for bond lengths and bond angles are 0.012 Å and 1.5°, respectively). The backbone conformation of 89.9% of the residues is within the most favored regions of the Ramachandran plot, with none in disallowed regions, as defined using PROCHECK (*37*). Coordinates and structure factors for this structure have been deposited in the Protein Data Bank (accession code 1LQF).

RESULTS

Structure−Activity Relationship of BzN−EJJ−Amide Analogues. To understand the chemical basis of the high potency of BzN−EJJ−amide (*20*), we synthesized and assayed several analogues of the inhibitor to determine structure−activity relationships. Results are summarized in Table 2. In comparison to the all *S*-isomer, the unnatural all *R*-isomer of BzN−EJJ−amide (Table 2, compound **2**) is over 200-fold less potent in inhibiting PTP-1B. This was not surprising as the all *R*-isomer, with the opposite stereochemistry at the Cα, would not be able to position the two phosphonates to make the required interactions. On the basis of published literature reports, it seemed likely that one of the phosphonates of BzN−EJJ−amide would bind at the active site, with the other moiety bound at the secondary aryl phosphate site delineated by Arg24 and Arg254 (*18*). Thus, it was of interest to determine how the other functional groups of the inhibitor influenced inhibitory potency.

We initially focused on the glutamic acid in the inhibitor, as most substrates of PTP-1B have an acidic amino acid that precedes the tyrosine that is dephosphorylated. To this end, the methyl ester analogue was synthesized and its effect on enzyme activity ascertained. The ester analogue (Table 2,

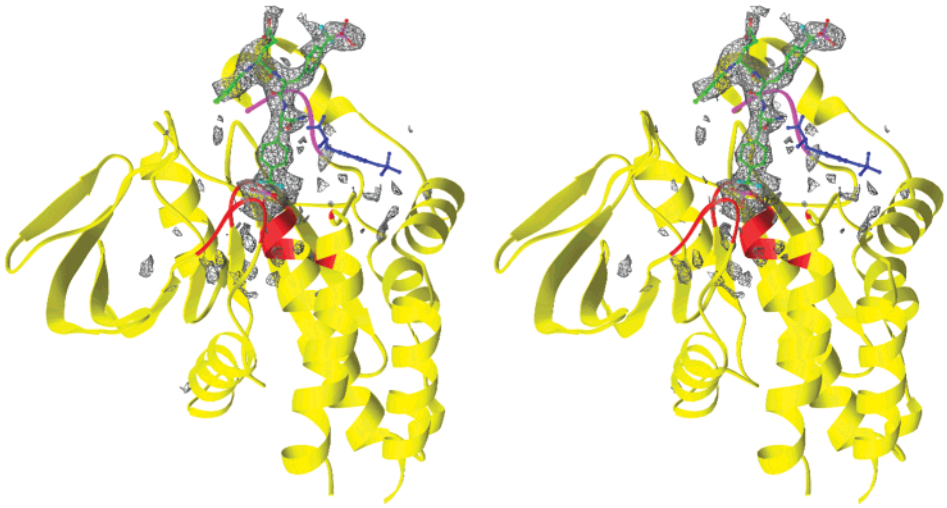

FIGURE 2: Stereoview of the (Fo−Fc) difference electron density map (contoured at 2σ) used to locate and orient BzN−EJJ−amide, together with the final model for the inhibitor and the ribbon diagram for PTP-1B. The secondary binding site is indicated by the presence of a second phosphotyrosine molecule (in blue, coordinates from 1PTY, overlaid with LSQMAN).

Table 2: Effect of BzN−EJJ−Amide Analogues on PTP-1B

inhibitor	stereochemistry	IC_{50} (nM)
BzN−EJJ−amide (**1**)	*S,S,S*	5 ± 2
BzN−EJJ−amide (**2**)	*R,R,R*	1010 ± 200
BzN−E(methyl ester)JJ−amide (**3**)	*S,S,S*	6 ± 1
BzN−GJJ−amide (**4**)	*S,S*	11 ± 1
EJJ−amide (**5**)	*S,S,S*	40 ± 4
BzN−EJJ−acid (**6**)	*S,S,S*	19 ± 2

compound **3**) was equipotent to the parent compound indicating that the negative charge of the carboxyl group was not crucial for inhibitor potency. This was an unexpected result, so we evaluated the importance of the glutamic acid side-chain for inhibitor potency by substituting it with glycine. The glycine analogue, BzN−GJJ−amide (Table 2, compound **4**), was about 2-fold less potent than the parent compound. Thus, although the presence of the negative charge is not required for inhibitory potency, the propionyl side chain provides additional binding energy. Next, we evaluated the contribution of the N-terminal benzoyl group to inhibitor potency. Removal of the benzoyl group (Table 2, compound **5**) resulted in a 5-fold less potent compound indicating that this group provides favorable interactions with the protein. Finally, the influence of the terminal amide group on inhibitor potency was assessed by replacing it with a carboxylic acid (Table 2, compound **6**). The introduction of the negative charge decreased the inhibitory potency of the compound by a factor of about 4.

Effect of BzN−EJJ−Amide on Mutants of PTP-1B. To gain an insight into the structural features on PTP-1B that may influence inhibitor potency, we introduced amino acid substitutions into the protein by site-directed mutagenesis. Our previous work (*20*) and other published reports (*38*, *39*) indicated that the YRD motif (residues 46−48) might be important for inhibitor potency and selectivity. Three single-site substitutions (R47K, D48N and D48A) were constructed and their kinetic parameters determined (Table 3). Substituting Arg47 with lysine (R47K) resulted in a protein that maintained a catalytic activity comparable to that of the wild-type protein with respect to hydrolysis of FDP and pNPP. Similarly, substituting aspartic acid for asparagine at position 48 (D48N) did not affect the catalytic activity of the protein.

Table 3: Kinetic Parameters of Wild-Type PTP-1B and Mutant Derivatives on PNPP and FDP

	pNPP		FDP	
protein	K_M (mM)	k_{cat} (s^{-1})	K_M (mM)	k_{cat} (s^{-1})
wild-type	0.6 ± 0.1	38 ± 5	12 ± 3	1.4 ± 0.3
R47K	0.5 ± 0.1	50 ± 8	19 ± 2	2.9 ± 0.5
D48A	0.3 ± 0.01	9 ± 1	8 ± 0.4	3.2 ± 0.7
D48N	0.5 ± 0.07	24 ± 6	12 ± 4	1.2 ± 0.5

Table 4: Inhibition of Wild-Type PTP-1B and Mutant Derivatives by BzN−EJJ−Amide

protein	IC_{50} (nM)
wild-type	5 ± 2
R47K	23 ± 5
D48A	650 ± 130
D48N	8 ± 2

The D48A derivative exhibited a tendency for a decrease in K_M for both substrates. This PTP-1B derivative also showed a lower k_{cat} for pNPP but not for FDP. On the basis of the generally accepted catalytic mechanism of PTP-1B, this residue is not expected to influence the dephosphorylation of the thiol-phosphate intermediate. Hence, the reason for the decrease in turnover for pNPP is not clear at the moment.

Having determined the kinetic parameters for the wild-type and mutant proteins, we evaluated the inhibitory potency of BzN−EJJ−amide on the mutant proteins (Table 4). Replacing Arg47 with lysine resulted in a 4−5-fold decrease in inhibitor potency. Thus, it seems that the hydrogen bonding capability of the positive charge rather than the charge per se is important. Substitution of the aspartic acid residue at position 48 with asparagine did not affect the inhibitory potency of the inhibitor on the enzyme. In contrast, an alanine replacement (D48A) led to a 100-fold decrease in the potency of BzN−EJJ−amide, suggesting that an acidic/polar side chain in this position on the enzyme is important in inhibitor binding.

Crystal Structure of FLAG-PTP-1B (1−283) in Complex with BzN−EJJ−Amide. To understand the structural basis for the changes observed in the structure−activity relationships and the site-directed mutagenesis studies, we deter-

Table 5: Pairwise RMSD in Å on Positions for Atoms of the Four Molecules Found in the Asymmetric Unit[a]

	monomer B		monomer C		monomer D	
	Ca	all	Ca	all	Ca	all
monomer A	0.444	0.816	0.603	1.051	0.499	0.876
monomer B	−	−	0.527	0.933	0.405	0.845
monomer C	−	−	−	−	0.548	0.847

[a] The superimposition matrix was calculated with LSQMAN.

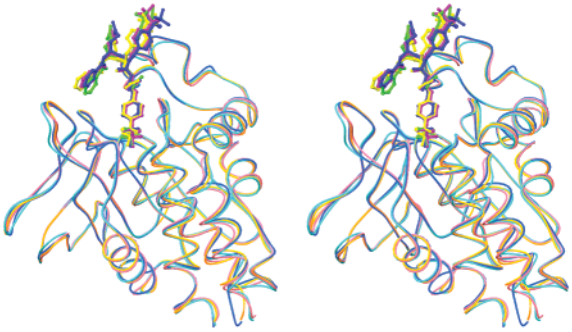

FIGURE 3: Stereoview of the four superimposed PTP-1B molecules found in the asymmetric unit. The four bound inhibitors are also displayed.

mined the crystal structure of PTP-1B in complex with BzN−EJJ−amide. The model contains four molecules per AU, each monomer including protein residues 1−283 and the four C-terminal residues of the FLAG, 506 water molecules, and 4 inhibitor molecules. The four monomers are very similar: Table 5 shows the pairwise RMSD for CA positions and all atom positions for the four monomers. The major differences are located at the N-termini and at surface loops spanning residues 60−64, 113−120, and 126−132 and are apparently due to differences in their respective packing environment. The inhibitor is bound in a very similar way in all four molecules (Figure 3), although there is a high degree of flexibility for the two N-terminal residues of the tripeptide. The C-terminal F_2PMP group of the tripeptide occupies the active site (Figure 4): the phosphonate oxygens are hydrogen bonded to the main-chain amide groups of the P-loop (spanning residues Ser216−Gly220) and the side chain nitrogens of Arg221. There is one ordered water molecule (present in all four molecules) that is hydrogen-bonded to the fluorine atoms of the inhibitor, to one of the oxygen atoms of the phosphonate, to the main-chain nitrogen of Phe182, and to the side chain nitrogen of Gln266. Hydrophobic interactions are present between the C-terminal benzyl ring of the inhibitor and the side chains of Phe182 and Tyr 46.

Surprisingly, the second F_2PMP is not bound at the secondary binding site, as it would have been expected based on the 1PTY structure (*18*), and the recently reported structure of PTP-1B in complex with the active segment of the insulin receptor kinase domain (*19*). The difference electron density maps clearly and unambiguosly indicated both the position and orientation of the bound inhibitor (Figure 2); there was no observable difference electron density in the secondary binding site. The second F_2PMP moiety and the N-terminal glutamic acid bind in a very solvent-exposed area near Arg47. A difluorophosphonate group of another bisphosphonate inhibitor of PTP-1B has recently also been observed to bind near Arg47 (*40*). Both

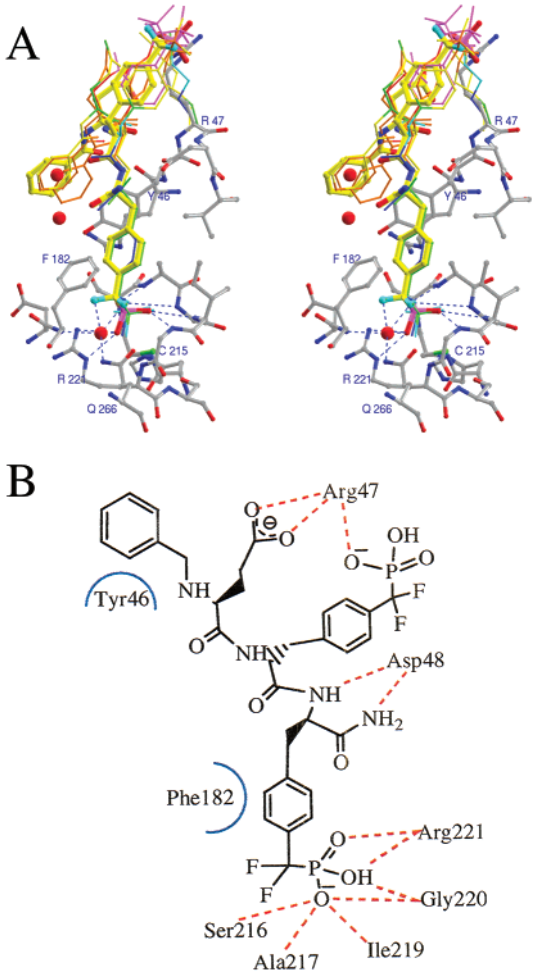

FIGURE 4: (A) Stereoview of BzN−EJJ−amide binding site in one of the four molecules (ball-and-stick colored according to atom color). Hydrogen bond interactions with atoms of the P-loop are indicated as dotted lines. The conformation for the other three inhibitors molecules, as well as those for the side chain of R47, are also displayed as thin bonds, colored according to temperature factors (temperature factors increasing: cyan, green, blue, yellow, orange, red, and magenta). (B) Schematic diagram of the residues interacting with the bound inhibitor. Hydrogen bond interactions are shown as red dotted lines, hydrophobic interactions as blue semicircles.

protein and inhibitor are characterized, in this area, by a very high degree of flexibility, as evident by the relatively high thermal factors and the fact that BzN−EJJ−amide assumes four different conformations in the four molecules (Figures 3 and 4A). Inhibitor mobility is accompanied by a high degree of variability in the position of the side chain of Arg47 (Figure 4A). BzN−EJJ−amide is a tripeptide, and interestingly, it binds as other four- or six-residue peptides, bearing a single phosphotyrosine group, have been shown to bind to PTP-1B (*39*) (Figure 5). The binding of BzN−EJJ−amide differs from that of the bisphosphorylated IR peptide (*19*), and this is discussed below.

DISCUSSION

The results presented in Tables 2−4, together with the crystal structure of PTP-1B in complex with BzN−EJJ−amide, define specific roles for the residues involved in inhibitor binding and provide a molecular basis for the potency and specificity observed for the compound. A

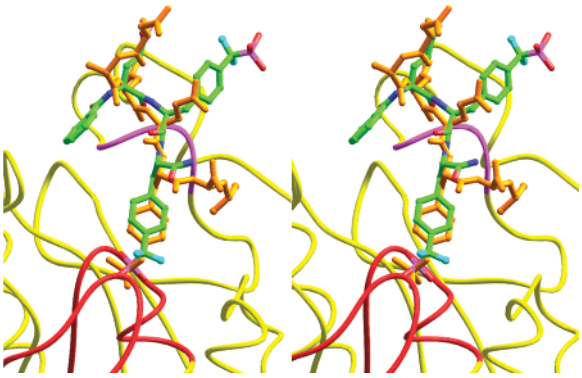

FIGURE 5: Stereoview of BzN−EJJ−amide overlaid onto a hexapeptide bound to PTP-1B (*39*). The conformations of the two ligands are very similar.

surprising but interesting revelation from the crystal structure is the binding orientation of the central F_2PMP moiety. This group binds in a solvent-exposed area close to Arg47. The side chain of Arg47 interacts with both the central F_2PMP and the N-terminal glutamic acid (see Figure 4). Modification of either the inhibitor (compound 4 in Table 2) or the protein (R47K) in this area affects the inhibitor binding, while the introduction of the methyl ester did not significantly affect the inhibitory potency of the resulting compound. Substitution of the glutamic acid moiety in the inhibitor with a glycine, or replacement of Arg47 with lysine, resulted in a loss of inhibitor potency. It seems likely that the positively charged ϵ-amino group (Nϵ) of lysine does not adequately replace the guanidinium group of Arg47. This area of the structure is characterized by a high degree of flexibility and therefore does not allow us to define specific atomic interactions between BzN−EJJ−amide and PTP-1B. However, it seems reasonable to suggest that a significant contribution to the binding energy derives from bidentate electrostatic interactions between the guanidinium group of Arg47 and the two N-terminal residues of the inhibitor (F_2-PMP and glutamic acid). The Nϵ of a lysine side chain would not be able to participate in such an interaction, thus potentially explaining the loss of potency observed for the R47K mutant. Another possible reason is that the lysine side chain in the mutant may assume a different position with respect to the one observed for the arginine in the WT enzyme.

The binding energy of BzN−EJJ−amide appears to result from several interactions with the protein that culminate in the substantial inhibitory potency against PTP-1B. As presented in Table 2, substitution of the glutamic acid with glycine, conversion of the terminal amide group to a carboxylic acid, or removal of the N-terminal benzoyl group all lead to a loss in inhibitor potency. The influence of the benzoyl group on inhibitor potency may be explained by its favorable van der Waals contacts with Phe46 in the YRD loop. This loop region, particularly residues 46−48 (the YRD motif), appears to play a crucial role in mediating several interactions with the inhibitor. In addition to mediating interactions with the benzoyl group and the second F_2PMP moiety (see above), interactions of the inhibitor with the YRD motif could also explain the loss of potency upon conversion of the C-terminal amide group to an acid (Table 2, compound 6). In the crystal structure, the C-terminal amide of BzN−EJJ−amide is hydrogen-bonded to the carboxyl side chain of Asp48. Ordinarily, a replacement of the amide with a carboxyl group would be expected to maintain hydrogen-bonding potential of the inhibitor. Hence, it seems likely that the 2-fold loss in inhibitor potency with the acid replacement may result from a more prominent contribution from electrostatic repulsion between the side chain of Asp48 and BzN−EJJ−acid.

As alluded to above, the terminal amide group of BzN−EJJ−amide is hydrogen-bonded to Asp48 via its carboxyl group. In addition, Asp48 is hydrogen-bonded to the main-chain nitrogen of the central F_2PMP group that is bound at the active site. As presented in Table 4, the potency of BzN−EJJ−amide on the D48N derivative of PTP-1B was comparable to that of the wild-type protein. In contrast, a 100-fold drop in potency was observed for the D48A derivative. Unlike the asparagine substitution (D48N) that is isosteric and preserves the hydrogen-bonding capability of the parental aspartic acid, an alanine substitution would be less complementary in shape and would have no hydrogen-bonding potential. Hence, this mutant would be expected to lose binding energy from both effects. The characterization of the PTP-1B mutants (Table 3) indicates that the amino acid substitutions did not drastically affect the kinetic parameters of the enzyme. Thus, the effects observed on the inhibitor appear to result from how these residues specifically interact with BzN−EJJ−amide.

The identification of a secondary aryl phosphate-binding site in PTP-1B suggested that this region of the protein could be targeted for the design of potent and selective inhibitors for this phosphatase (*18*). The importance of this secondary site is also demonstrated in the crystal structure of PTP-1B in complex with a peptide derived from the activation loop of the insulin receptor. This structure clearly indicates that the enzyme may indeed utilize the secondary aryl phosphate site to achieve substrate selectivity (*19*). Recently, Jia and colleagues have published the crystal structure of a nonpeptidic bisphosphonate in complex with PTP-1B (*40*). The authors observed that while one difluorophosphonate moiety was bound at the active site, the second group was not bound at the secondary binding site but rather close to Arg47. In this study, we find that a peptidic bisphosphonate inhibitor also binds close to Arg47 rather than at the secondary aryl phosphate-binding site. To obtain insights into the differential binding modes of the ligands, we have aligned the crystal structures of BzN−EJJ−amide (this study) and the IR peptide substrate (PDB entry 1G1H) (*19*) in Figure 6. Our discussion is restricted to the two pTyr residues (1162 and 1163) that are analogous to the F_2PMP groups of the inhibitor.

A comparison of the structures of BzN−EJJ−amide and the IR peptide in complex with PTP-1B shows that, although the primary sequence of both ligands are very similar (Figure 6), the structure-based alignment shows a one-residue frame shift. As a result, the more C-terminal F_2PMP group of the inhibitor is bound at the active site, whereas the analogous phosphotyrosine residue of the substrate is bound at the secondary aryl phosphate site. The more N-terminal or second F_2PMP binds in the P-1 position, with the glutamic acid occupying the P-2 position. BzN−EJJ−amide binds to PTP-1B in a manner similar to that of most peptide substrates which bear a single phosphotyrosine (cf the high affinity EGFR peptide, DADEpYL, shown in Figure 5; the sequence is also aligned with the BzN−EJJ−amide and the IR peptide

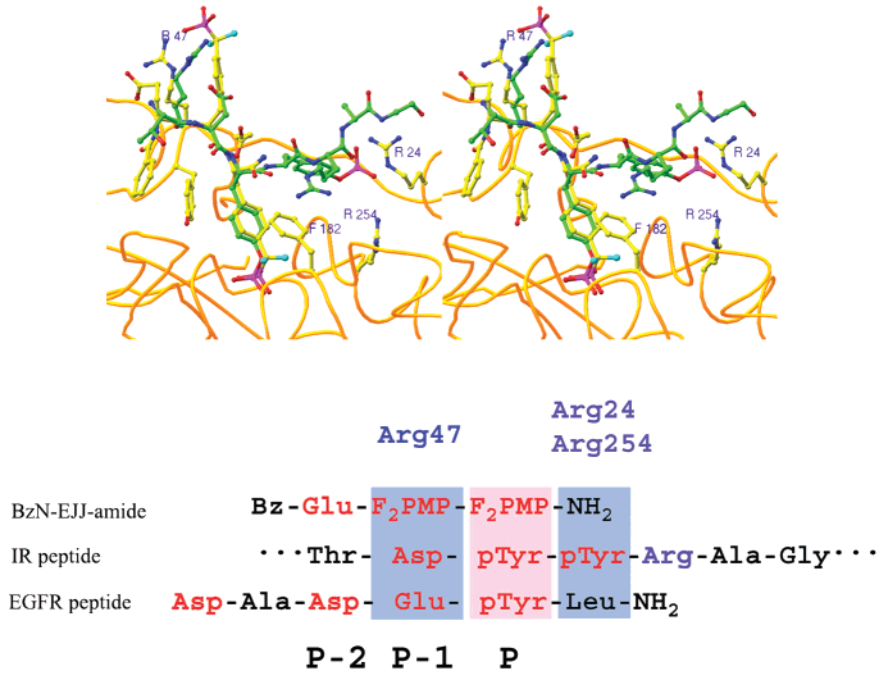

FIGURE 6: Stereoview of a bis-phosphorylated insulin receptor peptide bound to PTP-1B (PDB code 1G1H, green) overlaid onto the BzN−EJJ−amide:PTP-1B complex (yellow). Below is a schematic alignment of the sequences of BzN−EJJ−amide, the EGFR peptide (*39*), and the insulin receptor peptide (*19*); the residues are colored according to charge (red, negative; blue, positive; black, everything else). The composition of the peptide sequence before and after the pTyr likely determines the binding mode of the peptide itself. See text for a detailed discussion.

in Figure 6). It has been also shown that there is a strong preference for negatively charged residues in positions P-2 and P-1 and that, in the case of the P-1 site, this preference is directly determined by Arg47 (*20, 41*). Thus, we postulate that ligands with a sequence "acidic−acidic−pTyr" at the C-terminal end would bind as observed for the EGFR peptide and BzN−EJJ−amide in order to satisfy the binding preferences highlighted above. On the other hand, the presence of other residues C-terminal to the pTyr may contribute to the binding orientation of the ligand toward the secondary aryl phosphate site. An "inverse alanine scanning" approach has been used to demonstrate that residues beyond the P+1 position contribute to substrate recognition and efficacy (*42*). Interactions involving residues C-terminal to pTyr1162 and pTyr1163 with PTP-1B are observed in the structure of the IR peptide. Of special interest is the side chain of Arg1164, which forms a classic π-cation interaction with the side chain of Phe182 (*19*). These interactions are probably necessary and sufficient to orient the peptide substrate toward the secondary aryl phosphate-binding site. The sequence of the IR peptide visible in the complex is (1160)Thr−Asp−pTyr−pTyr−Arg−Ala−Gly(1166). If the IR peptide interacted with PTP-1B as discussed above for BzN−EJJ−amide, then pTyr1163 would be expected to bind at the active site. If this were the case, Arg1164 would be oriented toward the secondary binding site, where the presence of two arginine residues (Arg24 and Arg254) would engender an electrostatic repulsion. Additionally, Ala1165 would occupy the position observed for Arg1164; this would lead to a loss of the favorable interaction with the side chain of Phe182. Thus, the binding orientations observed for both ligands appear to maximize their interactions with the protein. The observed binding orientation of the IR peptide would therefore seem to be crucial for the preferential recognition of (E/D)−pY−pY−(R/K), a motif which has been demonstrated to be a consensus substrate recognition sequence for PTP-1B (*43*).

Our results confirm the alternative binding mode for small bisphosphonates reported by Jia et al. (*40*) and provide further evidence that targeting the YRD motif may result in potent and selective inhibitors for PTP-1B. It must be noted, however, that the high mobility of Arg47 may not readily facilitate the modeling of compounds targeting this residue. Asp48 seems more accessible, and work done to target this residue has been reported (*44*). A potential advantage that may result from targeting the YRD motif is that the approach may enable the synthesis of much simpler compounds rather than the bulky ones that are required to reach the secondary aryl phosphate binding site. However, our results suggest that analogues targeting both the YRD motif and the secondary aryl phosphate binding site could result in even more potent and selective inhibitors.

ACKNOWLEDGMENTS

We would like to express our gratitude to Dr. Kathleen Metters for her continued support and to the staff at beamline 17ID (APS) for their help during data collection.

REFERENCES

1. WHO. (1999) *Diabetes Mellitus*, WHO Fact Sheet 138.
2. Murphy, G. J., and Holder, J. C. (2000) PPAR-gamma agonists: therapeutic role in diabetes, inflammation and cancer, *Trends Pharmacol. Sci. 21*, 469−474.
3. Evans, J. L., and Jallal, B. (1999) Protein tyrosine phosphatases: their role in insulin action and potential as drug targets, *Exp. Opin. Invest. Drugs 8*, 139−160.
4. Elchebly, M., Payette, P., Michaliszyn, E., Cromlish, W., Collins, S., Loy, A. L., Normandin, D., Cheng, A., Himms-Hagen, J., Chan, C.-C., Ramachandran, C., Gresser, M. J., Tremblay, M. L., and Kennedy, B. P. (1999) Increased insulin sensitivity and obesity

resistance in mice lacking the protein tyrosine phosphatase 1B gene, *Science 283*, 1544−1548.
5. Klaman, L. D., Boss, O., Peroni, O. D., Kim, J. K., Martino, J. L., Zabolotny, J. M., Moghal, N., Lubkin, M., Kim, Y. B., Sharpe, A. H., Stricker-Krongrad, A., Shulman, G. I., Neel, B. G., and Kahn, B. B. (2000) Increased energy expenditure, decreased adiposity, and tissue-specific insulin sensitivity in protein-tyrosine phosphatase 1B-deficient mice., *Mol. Cell. Biol. 20*, 5479−5489.
6. Desmarais, S., Friesen, R. W., Zamboni, R., and Ramachandran, C. (1999) [Difluoro(phosphono)methyl]phenylalanine-containing inhibitors of protein tyrosine phosphatases, *Biochem. J. 337*, 219−223.
7. Taing, M., Keng, Y.-F., Shen, K., Wu, L., Lawrence, D. S., and Zhang, Z.-Y. (1999) Potent and highly selective inhibitors of Protein tyrosine-phosphatase 1B, *Biochemistry 38*, 2793−3803.
8. Andersen, H. S., Iversen, L. F., Jeppesen, C. B., Branner, S., Norris, K., Rasmussen, H. B., Moller, K. B., and Møller, N. P. (2000) 2-(oxalylamino)-benzoic acid is a general, competitive inhibitor of protein-tyrosine phosphatases, *J. Biol. Chem. 275*, 7101−7108.
9. Bleasdale, J. E., Ogg, D., Palazuk, B. J., Jacob, C. S., Swanson, M. L., Wang, X. Y., Thompson, D. P., Conradi, R. A., Mathews, W. R., Laborde, A. L., Stuchly, C. W., Heijbel, A., Bergdahl, K., Bannow, C. A., Smith, C. W., Svensson, C., Liljebris, C., Schostarez, H. J., May, P. D., Stevens, F. C., and Larsen, S. D. (2001) Small molecule peptidomimetics containing a novel phosphotyrosine bioisostere inhibit protein tyrosine phosphatase 1B and augment insulin action., *Biochemistry 40*, 5642−5654.
10. Kotoris, C. C., Chen, M. J., and Taylor, S. D. (1998) Novel phosphate mimetics for the design of nonpeptidyl inhibitors of protein tyrosine phosphatases, *Bioorg. Med. Chem. Lett. 8*, 3275−3280.
11. Larsen, S. D., Barf, T., Liljebris, C., May, P. D., Ogg, D., O'Sullivan, T. J., Palazuk, B. J., Schostarez, H. J., Stevens, F. C., and Bleasdale, J. E. (2002) Synthesis and biological activity of a novel class of small molecular weight peptidomimetic competitive inhibitors of protein tyrosine phosphatase 1B, *J. Med. Chem. 45*, 598−622.
12. Taylor, S. D., Kotoris, C. C., Dinaut, A. N., Wang, Q., Ramachandran, C., and Huang, Z. (1998) Potent non-peptidyl inhibitors of ptotein tyrosine phosphatase 1B, *Bioorg. Med. Chem. 6*, 1457−1468.
13. Wang, Q., Huang, Z., Ramachandran, C., Dinaut, A. N., and Taylor, S. D. (1998) Naphthalene-bis-[alpha, alpha-difluoromethylenephosphonates] as potent inhibitors of protein tyrosine phosphatases, *Bioorg. Med. Chem. Lett. 8*, 345−350.
14. Wrobel, J., Sredy, J., Moxham, C., Dietrich, A., Li, Z., Sawicki, D. R., Seestaller, L., Wu, L., Katz, A., Sullivan, D., Tio, C., and Zhang, Z.-Y. (1999) PTP1B inhibition and antihyperglycemic activity in the ob/ob mouse model of novel 11-arylbenzo[b]-naphtho[2,3-d]furans and 11-arylbenzo[b]naphtho[2,3-d]thiophenes, *J. Med. Chem. 42*, 3199−3202.
15. Xian, M., Wang, K., Chen, X., Hou, Y., McGill, A., Chen, X., Zhou, B., Zhang, Z.-Y., Cheng, J.-P., and Wang, P. G. (2000) Inhibition of protein tyrosine phosphatases by low-molecular-weight S-nitrosothiols and S-nitrosylated human serum albumin, *Biochem. Biophys. Res. Commun. 268*, 310−314.
16. Wrobel, J., Li, Z., Sredy, J., Sawicki, D. R., Seestaller, and L., Sullivan, D. (2000) Synthesis and PTP1B inhibition of novel 4-aryl-1-oxa-9-thiacyclopenta[b]fluorenes, *Bioorg. Med. Chem. Lett. 10*, 1535−1538.
17. Burke, T. R. J., Kole, H. K., and Roller, P. P. (1994) Potent inhibition of insulin receptor dephosphorylation by a hexamer peptide containing the phosphotyrosyl mimetic F2Pmp, *Biochem Biophys Res Commun. 204*, 129−134.
18. Puius, Y. A., Zhao, Y., Sullivan, M., Lawrence, D. S., Almo, S. C., and Zhang, Z.-Y. (1997) Identification of a second aryl phosphate-binding site in protein tyrosine-phosphatse 1B: a pardigm for inhibitor design, *Proc. Nat. Acad. Sci. U.S.A. 94*, 13420−13425.
19. Salmeen, A., Jannik N. Andersen, Micheal P. Meyers, Nicholas K. Tonks, and David Barford. (2000) Molecular Basis for dephosphorylation of the active segment of the insulin receptor by protein tyrosine phosphatase 1B, *Mol. Cell 6*, 1401−1412.
20. Asante-Appiah, E., Ball, K., Bateman, K., Skorey, K., Friesen, R., Desponts, C., Payette, P., Bayly, C., Zamboni, R., Scapin, G., Ramachandran, C., and Kennedy, B. P. (2001) The YRD motif is a major determinant of substrate and inhibitor specificity in T-cell protein-tyrosine phosphatase, *J. Biol. Chem. 276*, 26036−26043.
21. Skorey, K. I., Kennedy, B. P., Friesen, R. W., and Ramachandran, C. (2001) Develeopment of a robust scintillation proximity assay for protein tyrosine phosphatase 1B using the catalytically inactive (C215S) mutant, *Anal. Biochem. 291*, 269−278.
22. Ausubel, F. M., Brent, R., Kingston, R. E., Moore, D. D., Seidman, J. G., Smith, J. A., and Struhl, K. (1992) in *Short Protocols in Molecular Biology*, Green Publishing Associates/John Wiley and Sons, Inc., New York.
23. Otwinowski, Z., and Minor, W. (1997) Processing of x-ray diffraction data collected in oscillation mode, *Methods Enzymol. 276*, 307−326.
24. Howard, A. J. (2001) Data processing in Macromolecular Crystallography. in *Crystallographic Computing 7: Proceedings from the Macromolecular Crystallographic Computing School, 1996.* (P. E. Bourne and K. D. Watenpaugh, E., Ed.), Oxford University Press, Oxford.
25. Matthews, B. W. (1968) Solvent content of protein crystals, *J. Mol. Biol. 33*, 491−497.
26. Navaza, J. (1994) AMoRe: an automated package for molecular replacement, *Acta Crystallogr., Sect. A 50*, 157−163.
27. Brünger, A. T., Kuriyan, J., and Karplus, M. (1987) Crystallographic R-factor refinement by Molecular Dynamics, *Science 235*, 458−460.
28. Brünger, A. T. (1992) *X-PLOR Version 3 Manual: A System for Crystallography and NMR*, Yale University, New Haven, CT.
29. Brünger, A. T. (1992) The free-R value: a novel statistical quantity for assesing the accuracy of crystal structures, *Nature 355*, 472−474.
30. Roberts, A. L. U., and Brunger, A. T. (1995) Phase improvement by cross-validated Density Modification, *Acta Crystollagr., Sect. D 51*, 990−1002.
31. Kleyvegt, G. T., and Brunger, A. T. (1996) Checking your imagination: applications of the free R value, *Structure 4*, 897−904.
32. Jones, A. T., Zuo, J. Y., Cowan, S. W., and Kjeldgaard, M. (1991) Improved methods for building protein models in electron density maps and the location of errors in these models, *Acta Crystallogr., Sect. A 47*, 110−119.
33. Jones, A. T., & Kjeldgaard, M. (1997) Electron- density Map Interpretation, *Methods Enzymol. 277*, 173−208.
34. Collaborative Computational Project, N. (1994) The CCP4 suite: programs for protein crystallography, *Acta Crystallogr., Sect. D 50*, 760−763.
35. Brünger, A. T., Adams, P. D., Clore, G. M., DeLano, W. L., Gros, P., Grosse-Kunstleve, R. W., Jiang, J.-S., Kuszewski, J., Nilges, M., Pannu, N. S., Read, R. J., Rice, L. M., Simonson, T., and Warren, G. L. (1998) Crystallography & NMR system: a New Software Suite for Macromolecular Structure Determination, *Acta Crystallogr., Sect. D 54*, 905−921.
36. Rice, L. M., and Brunger, A. T. (1994) Torsion angle dynamics: Reduced variable conformational sampling enhances crystallographic structure refinement, *Proteins: Struct. Funct. Genet. 19*, 277−290.
37. Laskoswski, R. A., MacArthur, M. W., Moss, S. D., and Thornton, J. M. (1993) PROCHECK: a programme to check the stereochemical quality of protein structure coordinates, *J. Appl. Crystallogr. 26*, 283−291.
38. Sarmiento, M., Zhao, Y., Gordon, S. J., and Zhang, Z.-Y. (1998) Molecular basis for substrate specificity of protein tyrosine-phosphatase 1B, *J. Biol. Chem. 272*, 26368−26374.
39. Jia, Z., Barford, D., Flint, A. J., and Tonks, N. K. (1995) Structural basis for phosphotyrosine peptide recognition by protein tyrosine phosphatase 1B, *Science 268*, 1754−1758.
40. Jia, Z., Ye, Q., Dinaut, A. N., Wang, Q., Waddleton, D., Payette, P., Ramachandran, C., Kennedy, B., Hum, G., and Taylor, S. D. (2001) Structure of protein tyrosine phosphatase 1B in complex with inhibitors bearing two phosphotyrosine mimetics, *J. Med. Chem 44*, 4584−4594.
41. Sarmiento, M., Puius, Y. P., Vetter, S. W., Keng, Y.-F., Wu, L., Zhao, Y., Lawrence, D. S., Almo, S. C., and Zhang, Z.-Y. (2000) Structural basis of plasticity in protein tyrosine phosphatase 1b substrate recognition, *Biochemistry 39*, 8171−8179.
42. Vetter, S. W., Keng, Y. F., Lawrence, D. S., and Zhang, Z. Y. (2000) Assessment of protein-tyrosine phosphatase 1B substrate specificity using "inverse alanine scanning", *J. Biol. Chem. 275*, 2265−2268.
43. Myers, M. P., Andersen, J. N., Cheng, A., Tremblay, M. L., Horvath, C. M., Parisien, J. P., Salmeen, A., Barford, D., and

Tonks, N. K. (2001) TYK2 and JAK2 are substrates of protein-tyrosine phosphatase 1B, *J. Biol. Chem. 276*, 47771−47774.
44. Iversen, L. F., Andersen, H. S., Branner, S., Mortensen, S. B., Peters, G. H., Norris, K., Olsen, O. H., Jeppesen, C. B., Lundt, B. F., Ripka, W., Møller, K. B., and Møller, N. P. (2000) Structure-based design of a low molecular weight, nonphosphorus, nonpeptide, and highly selective inhibitor of protein-tyrosine phosphatase 1B, *J. Biol. Chem. 275*, 10300−10307.

BI0259554